

Beam profile sensitivity of the WMAP CMB power spectrum

U. Sawangwit^{*} and T. Shanks^{*}

Department of Physics, Durham University, South Road, Durham, DH1 3LE, UK.

31 May 2019

ABSTRACT

Using the published WMAP 5-year data, we first show how sensitive the WMAP power spectra are to the form of the WMAP beam. It is well known that the beam profile derived from observations of Jupiter is non-Gaussian and indeed extends, in the W band for example, well beyond its $12.6'$ FWHM core out to more than 1 degree in radius. This means that even though the core width corresponds to wavenumber $l \approx 1800$, the form of the beam still significantly affects the WMAP results even at $l \approx 200$ which is the scale of the first acoustic peak. The difference between the raw C_l and the de-beamed C_l is $\approx 70\%$ at the scale of the first peak rising to $\approx 400\%$ at the scale of the second.

New estimates of the Q, V and W-band beam profiles are then presented, based on a stacking analysis of the WMAP5 radio source catalogue and the WMAP5 temperature map. The radio sources show a significantly broader beam profile on scales of $10' - 30'$ than that found by the WMAP team whose beam analysis is based on measurements of Jupiter. Beyond these scales the beam profiles from the radio sources are too noisy to give useful information. Furthermore, we find evidence that fainter radio sources imply wider beam profiles than the brighter sources and also tentative evidence for a non-linear relation between WMAP and ATCA/IRAM 95 GHz source fluxes. We discuss whether the wide beam profiles could be caused either by radio source extension or clustering and find that neither explanation is likely. The reasons for the difference between the radio source and the Jupiter beam profiles are still unclear. If the radio source profiles were then used to define the WMAP beam, there could be a dramatic change in the amplitude and position of even the first acoustic peak. It is therefore important to identify the reasons for the differences between these two beam profile estimates.

Key words: cosmic microwave background – cosmology: observations

1 INTRODUCTION

The WMAP satellite has produced some of the best support for the standard Λ CDM cosmological model. By measuring the first two acoustic peaks it has shown that the Universe is spatially flat with $\Omega_\Lambda = 0.3$ and $H_0 = 72 \text{ kms}^{-1}\text{Mpc}^{-1}$ (Hinshaw et al. 2009). The precision of the fit is impressive and rules out many competing simple models such as the low H_0 , $\Omega_{\text{baryon}} = 1$ model of Shanks (1985, 2005, 2007).

Of course, statistically precise measurements can also contain systematic errors which have to be guarded against. Such systematics include Galactic foregrounds which at the least cause incomplete window functions on the sky (e.g. Bennett et al. 2003). There are also potentially more subtle systematics that arise from cosmological foregrounds. For example, Myers et al. (2004) and Bielby & Shanks (2007) have detected the SZ effect in the WMAP data by cross-correlating the CMB with rich cluster positions. Shanks (2007) has also discussed the effect of foreground lensing, prompted by QSO lensing results (Myers et al. 2003, 2005; Mountrichas & Shanks 2007). But SZ is unlikely to make a strong contribution to the first acoustic peak (Huffenberger et al. 2004).

Also lensing requires a high anti-bias between galaxies and the mass distribution to have a significant effect at the first peak which needs to be reconciled with measures of bias from galaxy clustering dynamics (e.g. Ratcliffe et al. 1998; Hawkins et al. 2003).

However, there are also many potential systematics involved with the WMAP instrument, although the WMAP team have taken care that the effects of such systematics are minimised. One major potential systematic concerns the question of the WMAP radio telescope beam profile. We shall see that even at the wavenumber $l \approx 220$ of the first acoustic peak, the CMB power spectrum has significant dependence on the beam profile even in the highest resolution 94GHz W band. Here the W-band resolution quoted by the WMAP team is $12.6'$ FWHM which is roughly equivalent to $l \approx 1800$. It is also noted that the beam is not Gaussian. Now the WMAP team have extensive papers devoted to the important question of measuring the beam (Page et al. 2003; Jarosik et al. 2007; Hill et al. 2009). The standard method is to use their observations of bright sources such as the planet Jupiter to measure the beam profile.

Here, after describing the WMAP5 data in §2, we re-derive in §3 the raw CMB power spectrum from the WMAP maps to show directly the effect of the beam. Then in §4 we use radio sources to make new estimates of the WMAP beam and discuss other tests of

^{*} E-mail: utane.sawangwit@durham.ac.uk, tom.shanks@durham.ac.uk

Table 1. Summary of the WMAP sources listed as point sources in the Greenbank and PMN 5GHz catalogues.

Band	$\geq 1.1\text{Jy}$	$< 1.1\text{Jy}$	Total ($> 2\sigma$)
Q	182	165	347
V	164	153	317
W	97	84	181

the beam profile. In §5 we then make fits to the radio source beam profiles and use these to de-beam the WMAP5 data and explore the range of power spectra that results. Possible reasons for the beam profile discrepancy and our conclusions are then presented in §6.

2 DATA

2.1 WMAP5 maps and point source catalogue

Here we use the five-year WMAP datasets which are available from the LAMBDA CMB website. The maps from the individual detectors in 5 frequency bands, K, Ka, Q, V (GHz) and W (94GHz) are supplied. The FWHM of the 94 GHz W beam is $12.6'$ compared to $19.8'$ at V (61 GHz), $29.4'$ at Q (41GHz), $37.2'$ at Ka (33GHz) and $49.2'$ at K (23GHz). There are 10 differencing assemblies (DAs), namely K1, Ka1, Q1, Q2, V1, V2, W1, W2, W3 and W4. The individual DA map can be cross-correlated to obtain power spectra free of uncorrelated detector noise bias (Hinshaw et al. 2003). The Jupiter beam profiles for each DA and the corresponding transfer functions are also given. The maps are in HEALPix (Górski et al. 2005) format with $N_{\text{side}} = 512$ and $N_{\text{side}} = 1024$. These give equal area pixels of dimension $\approx 7'$ and $\approx 3'$, respectively.

We use the 390 sources in the WMAP5 point source catalogue (Wright et al. 2009). These sources have to be detected to $> 5\sigma$ in at least one WMAP band and their flux density is reported if they are detected at $> 2\sigma$ in any of the other four WMAP bands, as long as the fitted source width is within a factor of 2 of the expected beam size. This gives a list of sources to about a limit of 0.5Jy in each band. The source positions are accurate to $\sim 4'$ (Wright et al. 2009). Table 1 shows the number of sources detected ($> 2\sigma$) in each band, also split into those brighter or fainter than 1.1Jy .

From the optical identifications of Trushkin (2003) of the 208 WMAP 1st year sources the survey contains 77 per cent QSOs or BL Lac with the remainder being radio galaxies/AGN. This is as expected given the dominance of flat-spectrum compact sources at the high WMAP frequencies. This is confirmed by inspecting the Green Bank list of counterparts at 5 GHz where only 30 out of 390 sources were found to be resolved at $4.6'$ FWHM resolution and these were then excluded from our WMAP point source list.

2.2 Ground-based 90-95GHz Radio Sources

We shall compare WMAP W-band fluxes with ground-based radio source fluxes from ATCA (Sadler et al. 2008) and IRAM (Steppe et al. 1988). The ATCA survey was made at 95 GHz and the IRAM survey at 90GHz. The ATCA survey was based on sources selected at 20GHz. Of the 130 sources observed, 17 were detected at more than 2σ by WMAP5. The IRAM survey observed 294 sources at 90 and 230 GHz, targeting sources which are brighter than 1Jy at 5 GHz. Here 66 sources were detected at more than 2σ by WMAP5. At these high frequencies the sources are mainly QSOs, BL Lacs or blazars. Many of the sources in the ATCA and IRAM surveys are variable and so where this is an issue

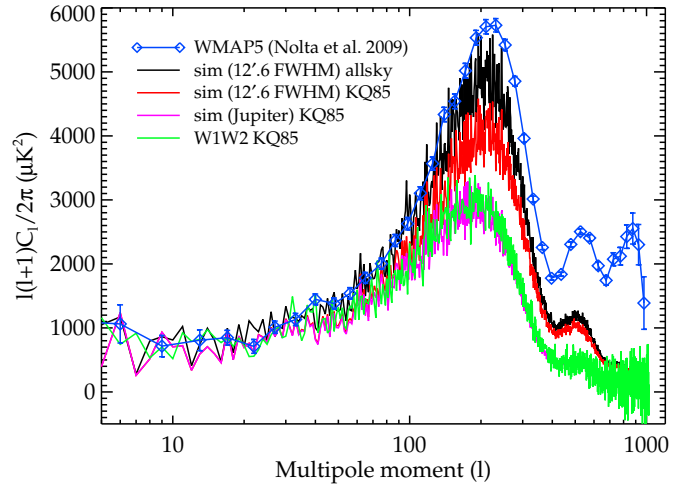


Figure 1. The raw CMB results from cross-correlating the W1 and W2 maps (green line) compared to the standard de-beamed WMAP result as presented by Nolte et al (blue line). Also shown are C_l measurements of an all-sky CMB simulation smoothed with a $12.6'$ FWHM Gaussian beam (black line), the same Gaussian smoothed map but with the KQ85 mask applied (red line) and a similar simulation now smoothed by the W1 and W2 Jupiter beams (magenta line). Although the raw CMB C_l (green) and the Jupiter beam-smoothed standard simulation C_l (magenta) agree, the difference between these and the Nolte et al result (blue) shows the large effect of debeaming even at the scale of the first acoustic peak.

we shall use the average source fluxes in our comparison with the WMAP fluxes.

3 DERIVING THE RAW C_l

We now analyse the WMAP W-band data to make an initial estimate of the power spectrum from the W band. To reduce the effect of correlated detector noise which would result from an auto-correlation of an individual CMB map, we make a cross-correlation of the maps from independent detectors. We derive the result by using the *anafast* code to cross-correlate the maps from the W1 and W2 detectors. In Fig. 1, we immediately see that the raw C_l (green line) is not only drastically smoothed at the position of the second and third peaks but there is also a significant effect at the position of the first peak at $l \approx 220$ in that the amplitude is now half of that expected for the standard ΛCDM result (blue line). The reason for this is seen in Fig. 2f where the beam profile from the Jupiter observations using the W1 detector are shown. It can be seen that the beam is not Gaussian and has a θ^{-3} power-law tail out to $> 1^\circ$.

Page et al. (2003) give the relation between the beam transfer function, b_l , and the radial beam profile, $b^S(\theta)$, as,

$$b_l = 2\pi \int b^S(\theta) P_l(\cos \theta) d \cos \theta / \Omega_B \quad (1)$$

The de-beamed cross-power spectrum measured from DA i and j is then given from the raw C'_l by

$$C_l = C'_l / b_i^i b_j^j p_l^2, \quad (2)$$

where p_l is the pixel transfer function supplied with the HEALPix package. For $N_{\text{side}} = 512$, the pixel window function lowers the raw C'_l by ≈ 1 and 10 per cent at $l \approx 200$ and 500, respectively.

If we use Eq. 2 with the Jupiter beam transfer function from the WMAP team, we find that we get close to the usual ΛCDM

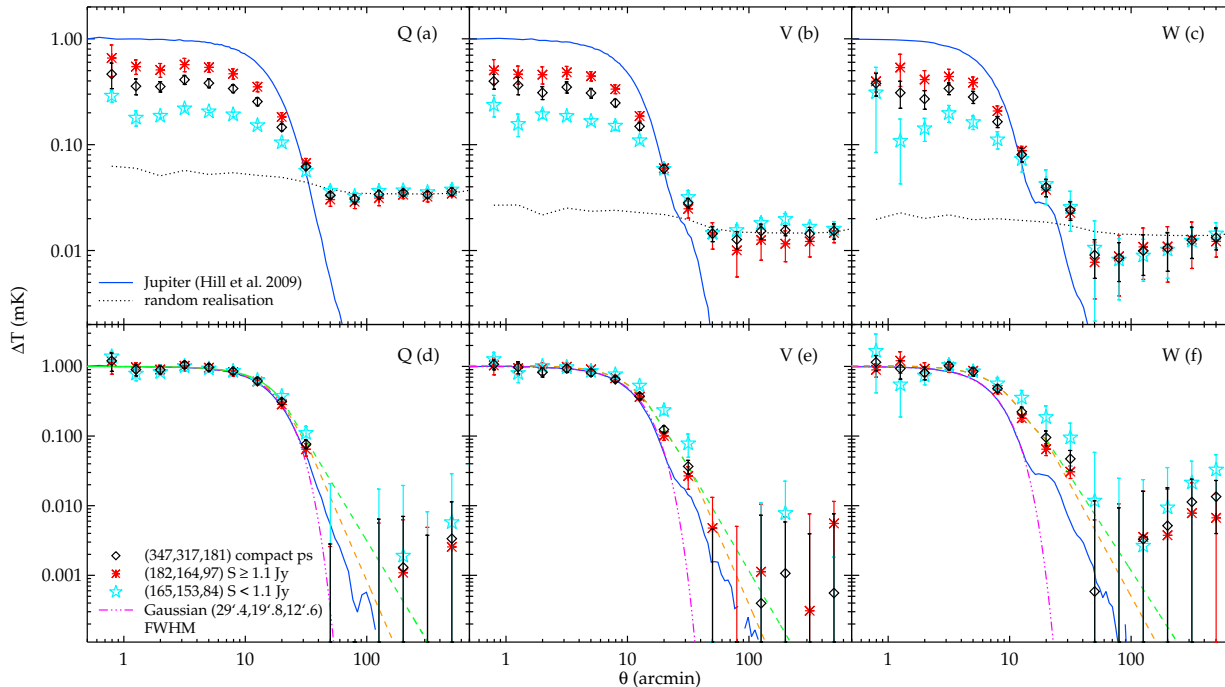


Figure 2. (a), (b) and (c); The raw radio source beam profiles for the WMAP sources compared to the beam profiles from Jupiter (solid lines) and random realisations (dotted lines) for Q1, V1 and W1. (d), (e) and (f); The zero-offset subtracted (see text) and normalised beam profiles for Q1, V1 and W1. The radio source profiles for all compact WMAP sources are shown as diamonds. Profiles derived from WMAP sources with flux brighter (fainter) than 1.1 Jy are shown as asterisks (stars). A Gaussian is shown as a dot-dashed line and empirical fits to the radio source profiles are shown as orange and green dashed lines.

model (green and orange lines in Fig. 4 below). The remaining discrepancy in the amplitude of the first peak is due to the incomplete sky coverage caused by the KQ85 mask. We have checked that this is the case using CMB simulations made using the *synfast* code supplied with the HEALPix software. Three simulation results are shown in Fig. 1. The black line shows the C_l measured from a full sky Λ CDM mock after smoothing by a Gaussian beam. The red line shows the C_l for a similarly smoothed Λ CDM mock cut by the KQ85 mask. Finally, the magenta line shows the effect of the W1W2 Jupiter beam smoothing a Λ CDM mock, again cut by the KQ85 mask. The latter shows excellent agreement with our cross-correlation of the W1, W2 maps cut by KQ85 whose C_l is shown by the green line. The effect of the Jupiter beam compared to the Gaussian beam is thus very significant in decreasing the height of the first peak. We also see that when the Jupiter beam and the appropriate mask is used, the Λ CDM model does give an accurate fit to the raw data C_l . So the difference between the raw C_l (green) and the WMAP5 (blue) results is $\approx 80\%$ due to the beam profile and $\approx 20\%$ due to the mask. Thus when we use the same parameters as the WMAP team, we reproduce the WMAP result.

4 TESTING THE WMAP BEAM PROFILE

4.1 Beam profiles via point sources

We then estimated a beam from the radio sources by making a stacking analysis of WMAP5 temperature maps around radio source positions. The extended foreground emission regions are excluded from the temperature maps using the ‘point source catalog mask’ (Wright et al. 2009). We calculated the average ΔT (per 49 arcmin² pixel) in annuli as a function of angular distance, θ , between radio source position and the pixel centre. In the first instance we show the raw cross-correlation function for the Q, V and

W bands in Fig. 2, split into bright (≥ 1.1 Jy) and faint (< 1.1 Jy) WMAP5 source sub-samples. The errors on the radio source profiles at each θ are *jackknife* errors based on 6 re-sampling fields. We see that the fainter source profiles appear to agree with the brighter source profiles at scales of $\theta \approx 30'$ but have significantly lower peak values. This is most clearly shown in the un-normalised profiles shown for the bright and faint Q, V, W band sources in Fig. 2a, b and c. This immediately suggests that there may be some form of non-linearity in the WMAP beam. However, we note that the profiles from both bright and faint sources show a positive offset at the 0.01-0.02 mK level. The offset shows an increasing trend from $1^\circ - 5^\circ$. The main uncertainty in estimating WMAP beam profiles from these data is in subtracting this offset at scales $> 1^\circ$. Note that the profiles and the associated errors remain roughly the same if we take the mean of all the sources rather than stacking them.

Since WMAP has significant sidelobes stretching to $\approx 90^\circ$ (Barnes et al. 2003), there was a possibility that the offsets are also part of the beam. However, when we distributed points at random in the masked region and used these as our centres for our stacking analysis we also found a similar offset (dotted lines in Fig. 2a, b and c). This makes it look like the offset is not associated with the existence of sources and hence not associated with the WMAP beam. We shall instead assume these offsets are caused by CMB fluctuations. However, there is still some ambiguity in at least the W band case, because when the offset estimated from the randoms is subtracted, the W band beam profile becomes negative at $\theta \approx 30'$. Clearly this is unphysical and may be caused by the presence of random background fluctuations local to the sources. We therefore have also employed a ‘photometry’ approach for the stacking analysis where we have subtracted the WMAP flux in an annulus at $1^\circ < \theta < 2^\circ$ for the W band and proportionately bigger annuli in the V and Q bands. Using sky annuli close to the sources will

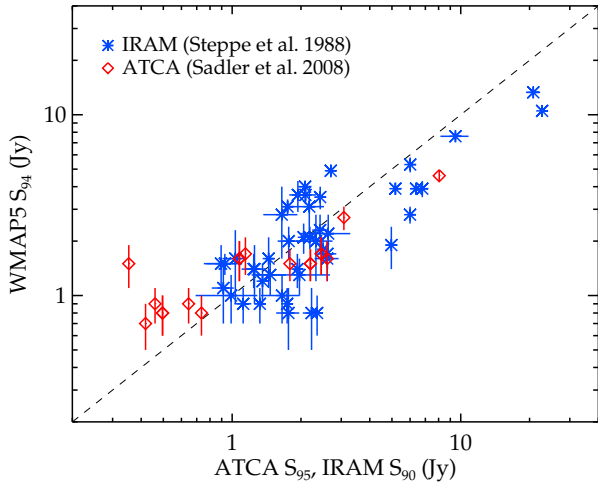


Figure 3. The comparison of the ATCA (diamonds) and IRAM (asterisks) source flux densities with the WMAP W-band data.

clearly improve background subtraction in the presence of local background fluctuations.

The resulting WMAP radio source beam profiles for Q, V and W bands are shown in Fig. 2d, e and f. The profiles have been renormalised to fit the peak in the WMAP Jupiter beam profile at $\theta < 4'$ and this profile is also shown. For each band we also compare the profiles to a Gaussian beam with the FWHM as indicated in the plot. We see that on average the profiles from the radio sources are broader than the Jupiter profile in the W, V and Q bands. In the lower frequency, lower resolution K and Ka bands the radio source profiles fit the Jupiter beam better, indeed almost perfectly (not shown here). Clearly, given the size of the errors there is little information from the radio sources on the beam profile at $\theta > 30'$. Fig. 2 again shows the WMAP radio sources divided into faint and bright sources, split at 1.1 Jy. In the W and V bands particularly we again note that the fainter sources appear to be wider than the brighter sources. When an offset estimated from the above random sampled points is subtracted from the stacked data, the profile widths slightly decrease but still show evidence for a significantly increased beam size over the Jupiter beam. These deviations from the WMAP Jupiter beam are puzzling and we now check to see if they could be caused by systematics.

We first checked the effect of pixelisation on the sources by using the smallest HEALPix pixels with $N_{\text{side}} = 1024$ (i.e. dimension $\sim 3'$). There were no differences seen in the results. Furthermore, the convolution with the $N_{\text{side}} = 512$ (as used here) pixel window function is too narrow to explain the discrepancy between the Jupiter beam of the WMAP team and our measurements.

We have checked the likely contribution of radio source clustering to the beam profiles, using the clustering analysis of the NVSS radio survey by Overzier et al. (2003). At $S \geq 200$ mJy where the sky density of NVSS sources is $n \approx 0.6 \text{ deg}^{-2}$,

$$w(\theta) = 3 \times 10^{-5} \theta^{-3.4} + 6.6 \times 10^{-3} \theta^{-0.8}. \quad (3)$$

This is a 2-power-law form which changes slope at $\theta \approx 0.1^\circ$. At smaller scales, double-lobed radio sources split into two components dominate while at larger scales source-source clustering dominates. We estimate the contribution of sources by first calculating the excess number of sources in an annulus of area ΔA at radius θ from an average source, $N_{\text{ex}}(\theta) = w(\theta)n\Delta A$. The excess flux/temperature per unit area in the profile in the annulus is then given by $\Delta T_{\text{ex}} = N_{\text{ex}} \times \bar{f}/\Delta A$ where \bar{f} is the average source

flux. For a Gaussian point source of central intensity/temperature per unit area, T_0 , and width, σ , the flux is $2\pi\sigma^2 T_0$. Therefore in this case, $\Delta T_{\text{ex}}(\theta) = w(\theta)2\pi n\sigma^2 T_0$. Substituting in the above values for n and w at $\theta = 0.5^\circ$ with $\sigma = 5.4'$ as for the W band we find $\Delta T_{\text{ex}} \approx 3 \times 10^{-4} T_0$ which is a negligible contribution in explaining the excess in Fig. 2f at this scale, if T_0 is taken to be the central profile value. Taking the parameters for 100 mJy from Overzier et al. (2003) makes the effect even smaller. These results are also likely to be upper limits for the WMAP sources which only have a density of $n \approx 0.01 \text{ deg}^{-2}$ and an average 95 GHz flux of 500 mJy. We conclude that radio source clustering is not likely to be an issue for our radio source beam profiles.

We conclude that in the W and V bands and probably also the Q band, the average radio source profile is wider than the Jupiter beam and the fainter sources show a wider profile than the brighter sources. This conclusion appears independent of the method of subtracting the offsets caused by CMB fluctuations.

4.2 Comparison with ground-based fluxes

Given the evidence that the WMAP beam profile is flux dependent, particularly in the W band, we now make a check of the WMAP5 W band fluxes as presented by Wright et al. (2009) in their Table 1. We checked these against the ATCA and IRAM source flux densities. The comparison in Fig. 3 shows that for both surveys, the brighter sources with fluxes > 3 Jy are about a factor of 1.5 fainter in the WMAP source list than in the ATCA or IRAM lists. The agreement between the ATCA and IRAM fluxes appears better than for WMAP, if we use WMAP as an intermediary between these two surveys. If the scale error is due to WMAP, then this might confirm the idea that there is a non-linearity in the WMAP flux scale. It could mean that the narrower WMAP beam at brighter fluxes is missing a significant amount of flux in the tail of the beam profile.

5 IMPACT ON THE DE-BEAMED C_l

Finally, we use the information from our radio source beam profiles to judge what the effect might be on the de-beamed WMAP C_l . Unfortunately we will have to extrapolate our radio source fits in the regime beyond $\sim 1^\circ$ out to 5° because of the large errors on the radio source beam profile in this range. We first make an extrapolation where we fit the small-scale beam profile points and then extrapolate continuing with the power-law as shown by the green dashed lines in Fig. 2d, e and f. We also made a more conservative extrapolation where we again fit the small-scale data but then extrapolate continuing parallel to the Jupiter beam profiles at large scales (orange dashed lines in Fig. 2d, e and f).

The range of the radio source de-beamed C_l is shown by the two red lines and two cyan lines (for W and V bands) in Fig. 4. The most conservative model is $\approx 40\%$ higher than the Jupiter de-beamed C_l (green and orange lines) at the scale of the first peak. But the most extreme model is now a factor of 2-3 higher even at $l = 220$ than the standard model power spectrum. We note that it has been possible to derive consistent C_l 's between the V, W (and Q) bands, although we accept that this is due to the freedom we have in extrapolating our radio source beam profiles beyond $\theta \approx 30'$. These de-beamed C_l would rise another $\approx 20\%$ if the mask window function was taken into account. It seems that if the radio sources are indicating a wider beam profile, then the systematic uncertainty in the beam at the largest scales will dominate the error budget of the C_l even at the scale of the first acoustic peak. These larger errors would then allow a wider range of cosmological models to be fitted.

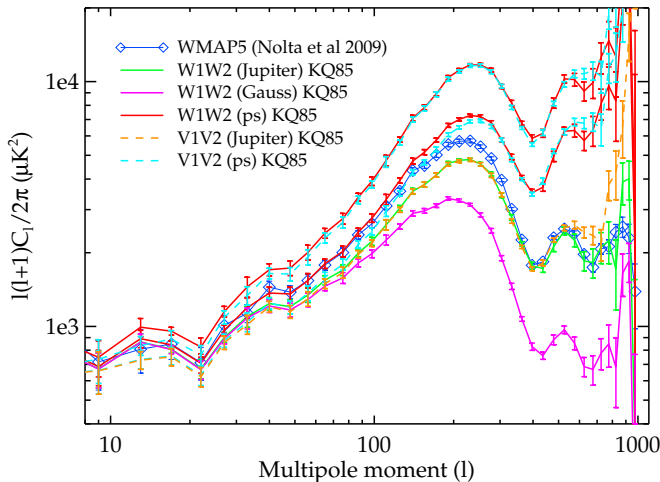


Figure 4. The de-beamed CMB power spectra. The blue diamonds show the standard WMAP result. The results from cross-correlating the W1 and W2 (V1 and V2) detectors and de-beaming with the Jupiter profile is shown as the green (orange) line - the difference with the standard result is due to the KQ85 mask. The same result but now de-beamed using the 12.6 Gaussian is shown as the magenta solid line, significantly different from the result using the Jupiter profile to de-beam. The same results but now using the profiles from the compact radio sources are shown as the red and cyan lines for W and V band respectively where the higher de-beamed amplitudes correspond to the wider profiles shown in Fig. 2e and 2f.

6 DISCUSSION AND CONCLUSIONS

Clearly it is important to understand why the radio source profiles are so wide in the Q, V and W bands. If there is a correlation between beam width and source flux then it will be wrong to use Jupiter to debeam the CMB power spectra because in the W band, for example, the ≈ 1 Jy radio sources are much closer to the ≈ 0.5 Jy rms flux of the CMB fluctuations than the 60 Jy flux of Jupiter.

The non-linearity shown by the WMAP source fluxes compared to independently measured ATCA/IRAM fluxes is powerful supporting evidence of non-linearity in the WMAP data calibration. It is possible that somehow the variability of the radio sources at W have caused problems that would not apply to the CMB. In passing, we note that the smaller than expected SZ decrements from WMAP observations of rich clusters (Myers et al. 2004; Bielby & Shanks 2007) may also be explained by a wider than expected WMAP beam at W. If so, this would argue that the non-linearity affects variable and non-variable WMAP sources alike.

In considering possible causes of WMAP non-linearity, we first note that detector saturation is unlikely to be the problem since this would lead to the brighter sources having a wider profile than the fainter sources, which is opposite to what is observed. However, Jupiter, being a moving source, has to be dealt with in a different way to the radio sources and the CMB fluctuations in the maps. This means that if there was a problem in the WMAP analysis, it would be necessary to check any filtering that is done to the maps.

In their Section 4, Hinshaw et al. (2009) state that a main goal of the WMAP data processing is to fit the calibration and sky signal simultaneously. They note that since the data model is nonlinear and the number of parameters is large, the general problem is intractable. They therefore proceed iteratively but it might be speculated whether there could be any issues with this iteration. Their Eq. 2 has $d_i = g_i(\Delta T_{vi} - \Delta T_{ai}) + b_i$, where d_i is the difference recorded between the two radiometer channels, g_i is the radiometer gain and b_i is a baseline that has to be fitted. ΔT_{vi} and

ΔT_{ai} are the true temperature differences from the dipole and the CMB fluctuations respectively. It is conceivable that badly fitting baselines and/or gains might lead to non-linearities with the radio source profiles. We conclude that;

- The WMAP power spectrum is heavily dependent on the beam profile. Indeed even the first acoustic peak at $l \approx 220$ is very dependent on the form of the profile at $1^\circ - 2^\circ$ where the profile is only ≈ 0.1 per cent of its peak value.
- The radio point sources detected by WMAP in the Q, V and W bands generally show a broader beam profile than the Jupiter beam used by the WMAP team.
- There is evidence for a flux dependent effect within the WMAP data in that fainter radio sources appear to have systematically broader profiles than brighter sources.
- Non-linearity in the WMAP flux scale may also be indicated by comparisons of WMAP radio source fluxes with ATCA and IRAM fluxes which show 50 per cent reduced flux from WMAP.
- If the Jupiter beam profile is systematically narrower than that shown by radio sources then their broader beam profile may be more appropriate for de-beaming the WMAP power spectrum.
- The systematic errors on the WMAP C_l due to the beam may be much larger than previously expected and in turn, this means that the systematic error on the best fit cosmological model may also be larger. It will be interesting to see if a revised estimate of the WMAP beam profile then allows a simpler cosmological model to be fitted than Λ CDM.

Acknowledgements: We acknowledge the use of NASA WMAP data. We thank G. Hinshaw and E. Wright for useful comments. US acknowledges financial support from the Royal Thai Government.

REFERENCES

- Barnes C., et al. 2003, ApJS, 148, 51
 Bennett C. L., et al. 2003, ApJS, 148, 97
 Bielby R. M., Shanks T., 2007, MNRAS, 382, 1196
 Górski K. M., et al. 2005, ApJ, 622, 759
 Hawkins E., et al. 2003, MNRAS, 346, 78
 Hill R. S., et al. 2009, ApJS, 180, 246
 Hinshaw G., et al. 2003, ApJS, 148, 135
 Hinshaw G., et al. 2009, ApJS, 180, 225
 Huffenberger K. M., Seljak U., Makarov A., 2004, Phys. Rev. D, 70, 063002
 Jarosik N., et al. 2007, ApJS, 170, 263
 Mountrichas G., Shanks T., 2007, MNRAS, 380, 113
 Myers A. D., et al. 2003, MNRAS, 342, 467
 Myers A. D., et al. 2004, MNRAS, 347, L67
 Myers A. D., et al. 2005, MNRAS, 359, 741
 Overzier R. A., Röttgering H. J. A., Rengelink R. B., Wilman R. J., 2003, A&A, 405, 53
 Page L., et al. 2003, ApJS, 148, 39
 Ratcliffe A., Shanks T., Parker Q. A., Fong R., 1998, MNRAS, 296, 191
 Sadler E. M., et al. 2008, MNRAS, 385, 1656
 Shanks T., 1985, Vistas in Astronomy, 28, 595
 Shanks T., 2005, in M. Colless, L. Staveley-Smith, & R. A. Sthakakis ed., Maps of the Cosmos Vol. 216 of IAU Symposium, Problems with the Current Cosmological Paradigm. pp 398–
 Shanks T., 2007, MNRAS, 376, 173
 Steppe H., et al. 1988, A&AS, 75, 317
 Trushkin S. A., 2003, Bull. Special Astrophys. Obs., 55, 90

